

# First Results From MAST

A.Sykes, representing the MAST team

EURATOM/UKAEA Fusion Association, Culham Science Centre, Abingdon,  
Oxfordshire, OX14 3DB

e-mail contact: [alan.sykes@ukaea.org.uk](mailto:alan.sykes@ukaea.org.uk)

**Abstract.** MAST is one of the new generation of large, purpose-built Spherical Tokamaks now becoming operational, designed to investigate the properties of the ST in large, collisionless plasmas. The first 6 months of MAST operations have been remarkably successful. Operationally, both merging-compression and the more usual solenoid induction schemes have been demonstrated, the former providing over 400kA of plasma current with no demand on solenoid flux. Good vacuum conditions and operational conditions, particularly after boronisation in trimethylated boron, have provided plasma current of over 1MA with central plasma temperatures (Ohmic) of order 1keV. The Hugill and Greenwald limits can be exceeded, and H-mode achieved at modest additional NBI power. Moreover, particle and energy confinement show an immediate increase at the L-H transition, unlike START where this only became apparent at the highest plasma currents. Halo currents are small, with low toroidal peaking factors, in accordance with theoretical predictions, and there is evidence of a resilience to the major disruption.

## 1. Introduction

The MAST device now operational at Culham is essentially a scaled-up version of the successful START experiment [1] but with better vacuum conditions, feed-back controlled power supplies, and having a plasma cross-section comparable to ASDEX-U and DIII-D. Key parameters of MAST and START are compared in Table 1.

|                                     | MAST       |           | START (achieved) |
|-------------------------------------|------------|-----------|------------------|
|                                     | Design     | Achieved  |                  |
| Minor & Major radii a,R (m)         | 0.65, 0.85 | 0.65,0.85 | 0.25, 0.32       |
| $\kappa$ (elongation)               | $\leq 3$   | 2.2       | $\leq 3$         |
| Aspect Ratio (R/a)                  | $\geq 1.3$ | 1.3       | $\geq 1.2$       |
| Plasma & TF rod current (MA)        | 2, 2.2     | 1.05 2.1  | 0.31, 0.5        |
| Toroidal field at R (Tesla)         | 0.52       | 0.51      | 0.31             |
| Aux. Heating: $P_{\text{NBI}}$ (MW) | 5          | 1         | 1                |
| $P_{\text{ECRH}}$ (MW)              | 1.5        | 0.6       | 0.2              |
| Pulse length                        | 1 – 5s     | 0.5       | $\leq 0.06$ s    |
| Bake-out temp ( $^{\circ}$ C)       | 200        | 140       | 50               |
| Plasma volume ( $\text{m}^3$ )      | 10         | 10        | 0.5              |

*Table 1 Comparison of key design parameters for MAST and START*

MAST achieved first plasma in December 1998. Since that time the central solenoid has been re-wound with improved insulation, a fully instrumented centre column has been fitted, and the two beam-lines on loan from ORNL have been installed and operation at up to 1MW demonstrated. Extensive internal diagnostics have been installed to provide accurate magnetic reconstruction (with EFIT), measure halo currents, divertor target parameters, etc.

## 2. Plasma Induction.

The plasma physics programme commenced in December 1999 with tests of the novel merging-compression technique whereby ST plasmas can be produced without the need of any flux from the central solenoid. This technique, pioneered on START utilises a special feature of the START and MAST designs, namely that the PF coils are inside the vacuum vessel as shown in Fig 1. The process involves the use of flux from the large-radius P3 coils, rather than the central solenoid (P1), to initiate the plasma. The toroidal field is applied, and initial deuterium gas injected into the tank. A large current is passed through the P3 coils and rapidly ramped down.

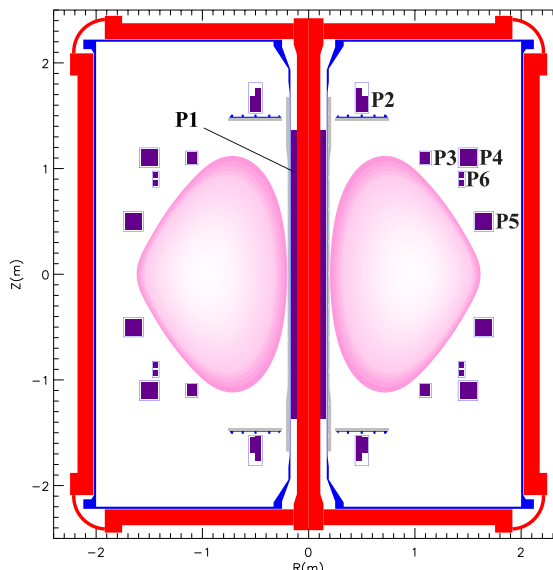


Fig 1 Plan view of MAST, showing the PF coils

Breakdown occurs in the form of plasma rings around each P3 coil. The plasma rings attract and merge on the midplane as the P3 current reduces toward zero. Application of a vertical field from the P4, P5 coils then compresses the plasma into the required ST configuration. Spherical Tokamak plasmas at currents of up to 450kA are routinely obtained by this merging-compression technique. The process is shown in Fig 2.

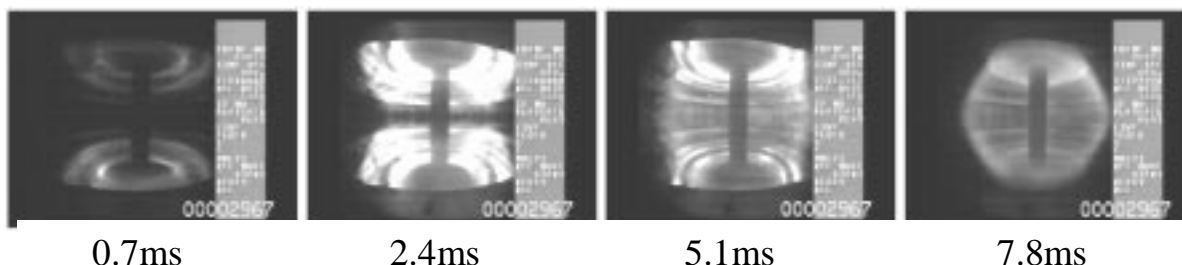
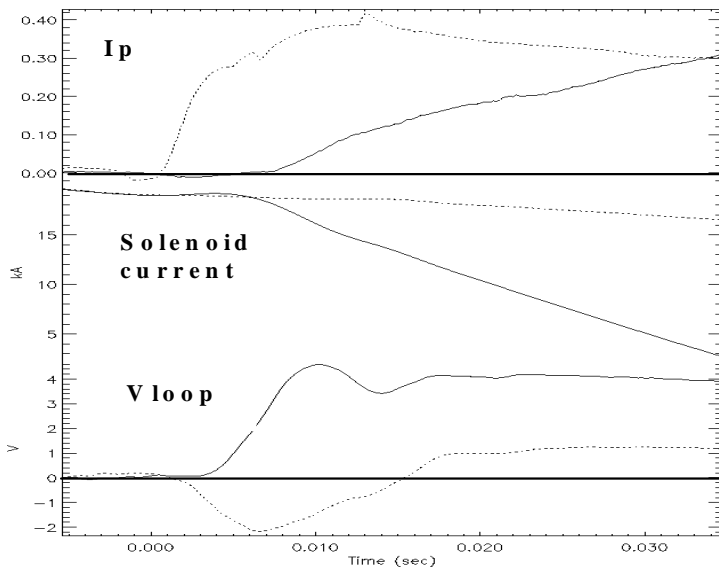


Fig 2 Stills from a high-speed video showing plasma formation by 'merging compression' in MAST #2967; times shown indicate elapsed time after ramp - down begins

The merging - compression scheme (#2967) is compared with the more conventional 'direct induction' scheme (#2898) in Fig 3. (It is important to note that, in this first campaign, the solenoid waveform is pre-set and not feed-back controlled). In 'direct induction' breakdown occurs in a poloidal field null, and sufficient electric field is provided by ramp-down of the solenoid current. The oscillations in loop voltage at the time of breakdown, present in both cases but larger in #2967, result from transient currents induced in the poloidal field coil cases. The stills shown in Fig 2 may be referred to the waveform for #2967 shown in Fig 3.

The merging-compression scheme is normally employed on MAST. After the spherical tokamak plasma has been established, the central solenoid is then used to maintain or

further increase the initial plasma current; plasma ramp rates of up to 13MA/s at a loop voltage of 7V can be achieved.



*Fig 3: 'direct induction' and 'merging - compression' schemes compared.*

*In 'direct' shot 2898 (full lines), the solenoid current is ramped down to give an initial loop voltage of 4V, which produces a plasma current ramp of ~9MA/s.*

*In merging-compression shot 2967 (dotted lines), the process produces 400kA of plasma current before the solenoid ramp begins; the low ramp rate giving  $V_{loop} \sim 1V$  is sufficient to maintain the plasma current*

Double null divertor (DND) plasmas of up to 1MA have been obtained using less than one-half of the designed maximum flux swing of approx. 1Vs. Discharge #2482 (May 2000) obtained over 1MA (Fig 4) using ~0.4Vs. The plasma had elongation ~ 2, and an overall diameter of approx. 2.6metres. Heated by NBI power of ~650kW, the plasma attained central electron and ion temperatures of over 1keV.

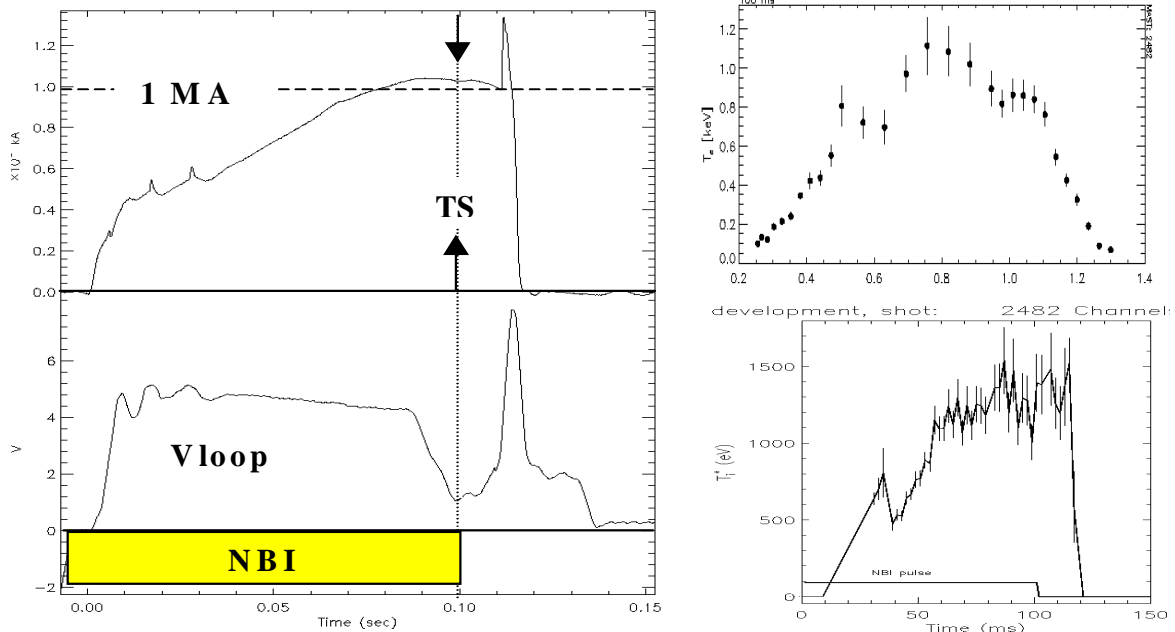


*Fig 4 First 1MA plasma on MAST, May 2000. As in all discharges during this first campaign, the solenoid waveform is pre-set and not feed-back controlled. The TS profile shows central electron temperature ~1keV, the NPA signal indicates central ion temperature ~ 1keV*

### 3. Plasma Conditioning

Vacuum conditions on MAST have been further improved by ‘boronisation’, whereby a thin layer of boron is deposited over material surfaces by glow cleaning in a mixture of deuterated trimethyl boron and helium. A ten-fold reduction in impurity emission was achieved (Fig 5), and the plasma current obtained increased by 20% for the same loop voltage waveform.

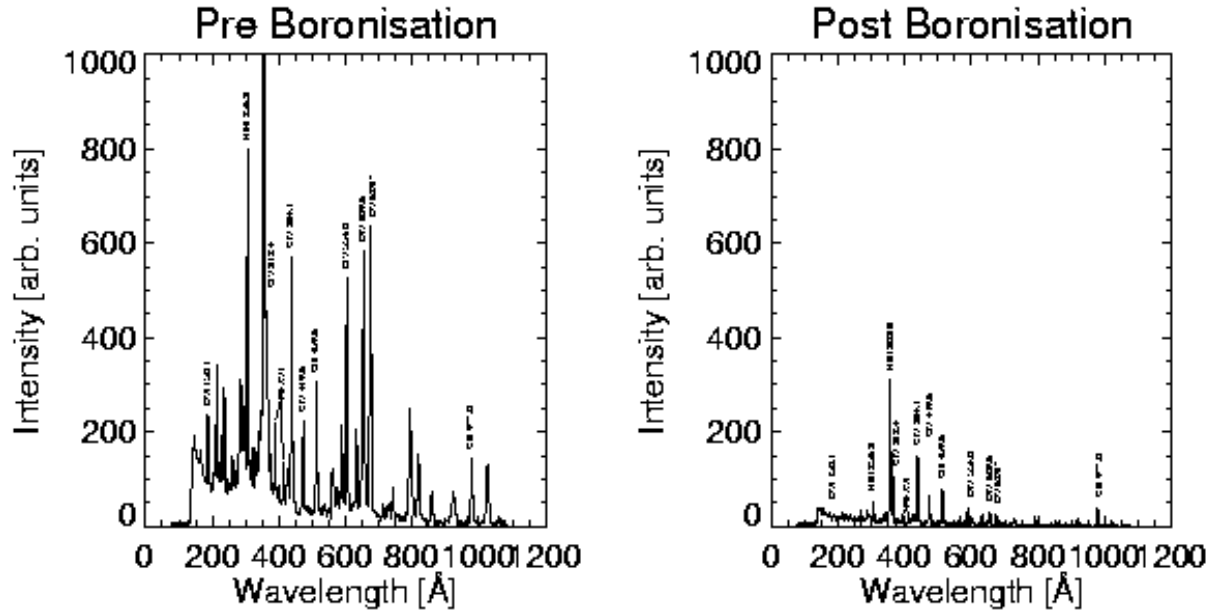
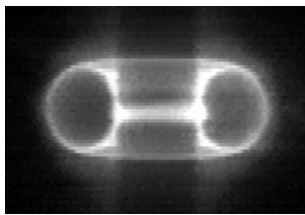


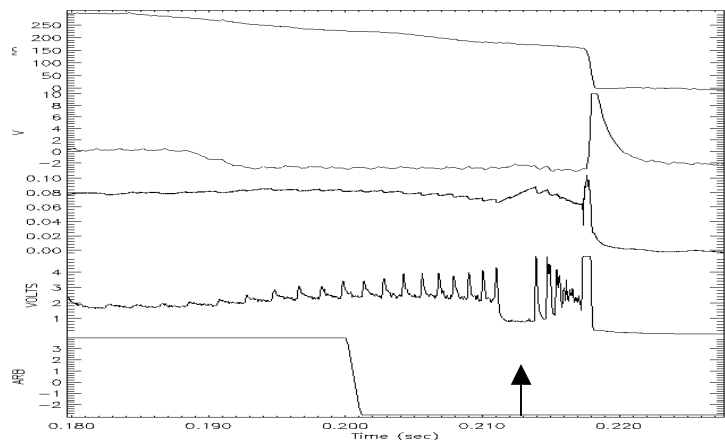
Fig 5 Plasma impurity fractions immediately before and after the first boronisation of MAST

Following the first boronisation, the first H-modes were observed in Ohmic plasmas. These were limited on the centre-column graphite, and occurred during the current decay phase when the aspect ratio was relatively large (Fig 6) – illustrating that conventional aspect ratio plasmas can also be studied in MAST.



Video image at  $t=0.213s$  (arrowed)

Fig 6 Observation of H-mode during current ramp-down in Ohmic MAST shot 2821. The plasma aspect ratio at this time is  $A=2.1$  ( $a\sim 0.18m$ ,  $R\sim 0.38m$ )



## 4. Neutral Beam Injection

MAST is equipped with two NBI lines on loan from ORNL. At full specification, they are together designed to deliver 5MW of 70keV deuterium. During the first campaign, the South injector alone was operational and capable of delivering up to 800kW of 30keV hydrogen.

Although this power and energy was very similar to that employed on START, beam heating (and current drive) are predicted to be more effective on MAST due to the higher fields and temperatures and larger plasma size: typical results of beam modelling, using the LOCUST Monte Carlo code, are shown in Fig 7. It is seen that the orbit in START is less well confined and leaves the plasma LCFS.

An E||B Neutral Particle Analyser (NPA), on loan from PPPL, has been installed at a tangency radius of 0.7m to diagnose the fast ion population resulting from NBI injection, and measure changes in the bulk thermal plasma temperature. The NPA can measure H and D particle energies from 0.5 to 600keV / amu for both H and D.

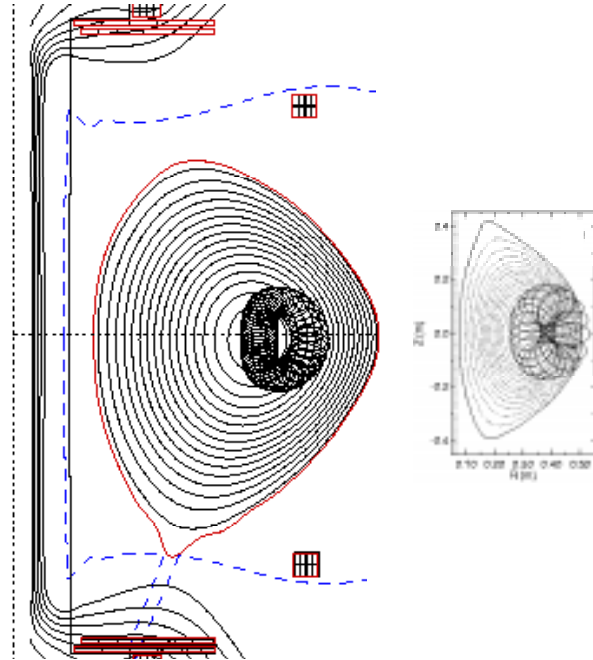


Fig 7 Comparison of 30keV H orbits modelled by the LOCUST Monte-Carlo code, in typical plasmas in MAST (left) and START (same scale)

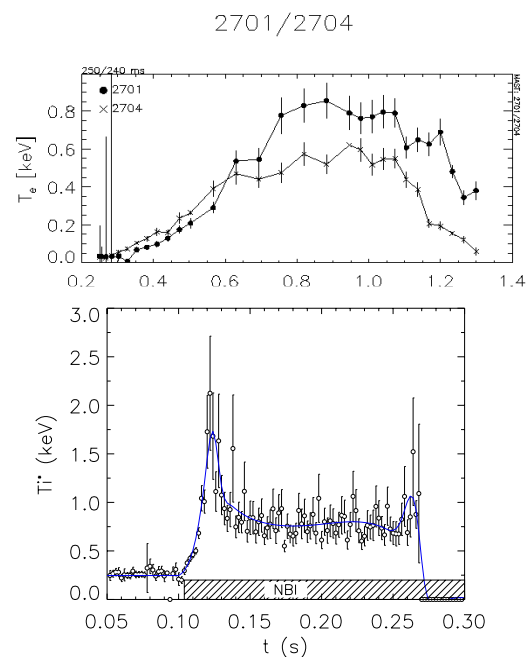
### 4.1 NBI heating on MAST

Heating of both electrons and ions is observed [2]. For example, the pair of discharges ~2701, 2704 are nominally identical except that 2701 had NBI heating of ~ 530kW at 30keV, whereas #2704 was Ohmic. The electron temperature profiles and the development of the central ion temperature are shown in Fig 8

In NBI heated #2701, the auxiliary heating was applied from 0.05s to 0.25s, at the end of this time the plasma thermal energy was double that in Ohmic discharge #2704. This increase in pressure produced the increase in plasma size seen in the  $T_e$  profile (the outer edge of the plasma extending beyond the range of the TS diagnostic).

Fig 8 (top) NBI heating of electrons (measured by 30-point Thomson scattering ) is shown by comparing NBI shot #2701 with the companion Ohmic discharge #2704

(below) in #2700 the central ion temperature (estimated from the NPA) increases from 300 to 700eV after NBI.



Still further increases in stored energy are obtained if an L-H transition occurs, as discussed in the next section.

## 4.2 H-mode Operation

First H-modes at low aspect ratio were achieved in NBI heated plasmas in June 2000 [3]. The transition to H-mode in MAST is clearly demonstrated in the pair of consecutive discharges 2700, 2701 shown in Fig 9. These had nominally identical parameters and appeared identical discharges until  $t = 220\text{ms}$  – so much so that the sawteeth crashes almost coincide. However #2700 achieved L-H transition, #2701 did not. These shots were part of a sequence of repeated shots: the next shot to achieve L-H transition was #2705. For these low power ( $\sim 530\text{kW}$ ) NBI heated discharges, transition appears to be a random occurrence; if it does occur it always follows a sawtooth crash.

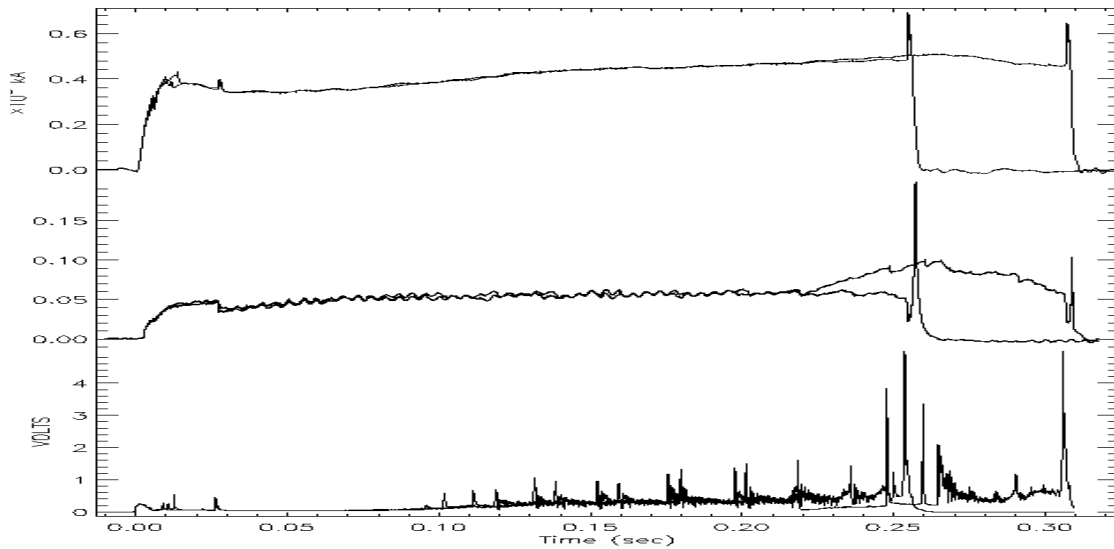


*Fig 9 Waveforms of #2700 (L-H transition at 0.22s) and #2701 (identical expt. parameters, but no transition). Both discharges end in a VDE*

Although the transition is achieved at relatively low NBI power, the total (Ohmic + NBI) power is typically 1.2MW, which is a factor of  $\sim 30$  greater than the threshold power for L – H transition predicted by the usual scalings [4]. This was also the case in START [5] but may indicate non-optimal operational conditions rather than an inadequacy in the scaling law. Although some periods of regular ELMing have been observed in MAST discharges, most H-mode discharges feature ELM-free periods (of up to 60ms) separated by giant ELMs, each ELM reducing the stored energy by up to 10% as shown in Fig 11.

## 5. Energy Confinement

In START, both L mode and H-mode confinement data is well represented by the ITER98pby1 scaling [1]. H-mode discharges only exhibited a clear improvement in confinement (compared to similar L-mode discharges) at the highest plasma currents ( $> 250\text{kA}$ ) achievable on START [5]. ELMy H-mode confinement data has been submitted to the International Database and is compared with confinement in world tokamaks in Fig 10.

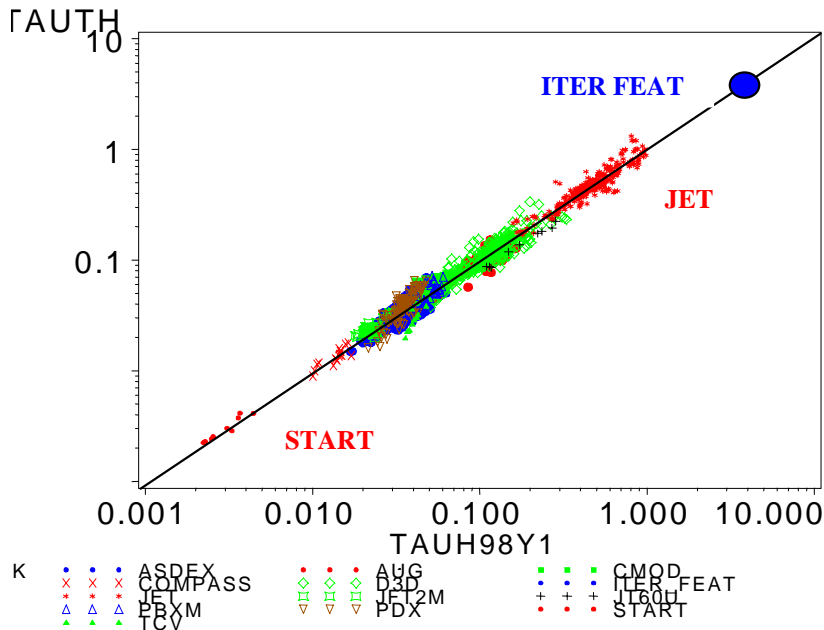


Fig 10 World tokamak ELMy H-mode confinement data, compared with the ITER98pby1 scaling

By using a combination of magnetic reconstruction provided by EFIT and kinetic evaluations using Thomson scattering and NPA diagnostics, confinement has been estimated in a range of MAST discharges. Of particular interest is the change in confinement at the L-H transition. In the steady L-mode period before transition to H-mode in #2700 the energy confinement is estimated to be  $\sim 14$ ms, compared to a prediction of 19ms given by I98pby1 scaling. After L-H transition a rapid increase in plasma thermal energy takes place, as shown in Fig 11.

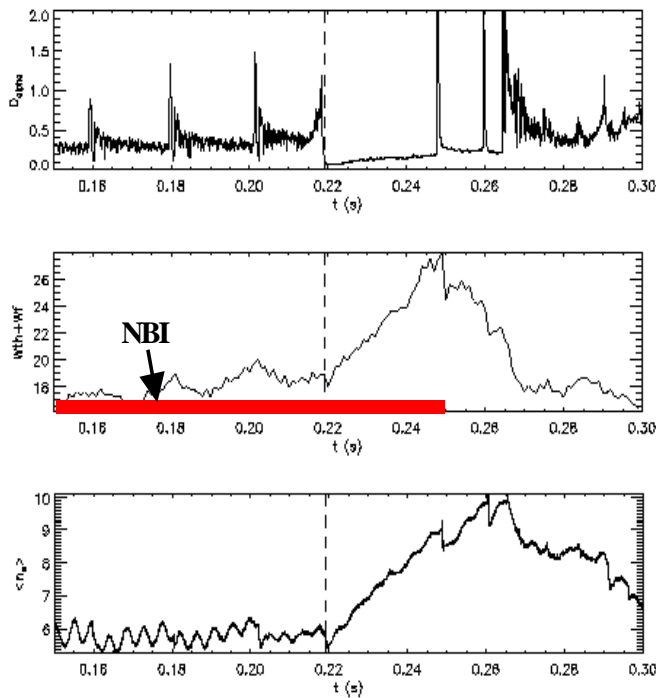


Fig 11 Detail of L-H transition on MAST #2700, showing mid-plane  $D\alpha$  emission, the plasma stored energy (including fast ion component), and the line integral density

Accurate evaluation of confinement after the transition is difficult due to the profile and plasma size changes accompanying the transition. Averaging over the period 218 – 250ms (at which point the NBI is shut off), and subtracting an estimate of the fast ion

contribution, a conservative estimate (evaluated at the centre of the period) is 34ms compared to an I98pby1 prediction of 25ms, an H-factor relative to I98pby1 of 1.4. This period includes a giant ELM. Although preliminary, these results indicate substantial improvements in confinement in H-mode even at these low plasma currents. Modelling suggests [6] that this difference from START is due to the very high neutral density present in START. This caused increased charge-exchange losses at transition, whereas in MAST the neutral density is typically 50 times lower, due mainly to the increased particle confinement time in the larger device.

## 6. Density Limits

MAST discharges can exceed the Hugill and Greenwald limits especially at low currents. These limits are here defined as  $n_H = I_p(MA) / (\pi a^2 \kappa)$  and  $n_G = I_p / (\pi a^2)$  respectively where  $n_H$ ,  $n_G$  are line average densities in units of  $10^{20} m^{-3}$ . By taking  $\kappa = 1.8$  (typical of MAST DND discharges) they can be compared on a single plot (Fig 12).

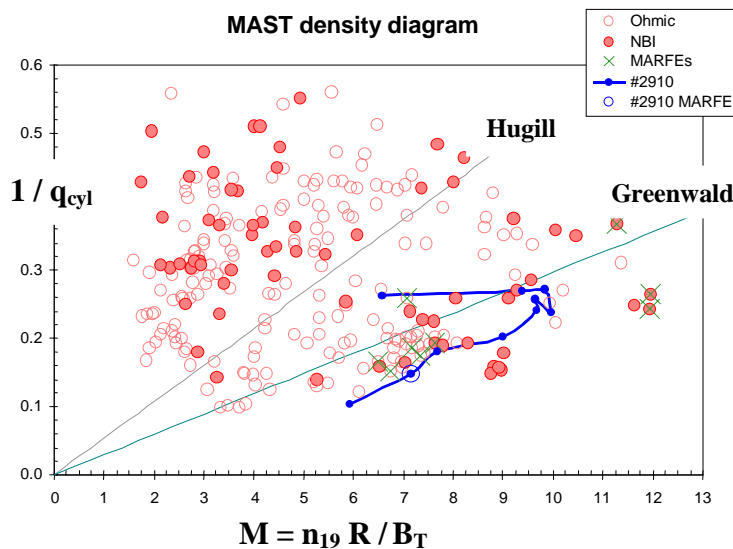


Fig 12 Operation space for MAST Ohmic and NBI discharges (summer 2000). Assumes  $q_{cyl} = 2.5 a^2 (1 + \kappa^2) B_T / R I_p$  and  $\kappa = 1.8$

It is seen that although the highest density shots have NBI heating, there is not a marked difference between Ohmic and NBI heated discharges (at least for these relatively low power NBI discharges) and several Ohmic shots exceed the Greenwald limit.

The trace in Fig 12 shows the time evolution of #2910, which had relatively high NBI power  $\sim 770kW$  and attained Greenwald number  $G \sim 1.4$  ( $G = n / n_G$ ). This shot had a MARFE at the time circled (evidenced on visual diagnostics as a toroidally symmetric ring of light on the centre column, which moved past the mid-plane, giving a 'blip' on the mid-plane interferometer). Other discharges exhibiting MARFEs, which on MAST have so far occurred close to the Greenwald limit, are shown as crosses in Fig 12; the MARFEs are transient, and do not cause radiation collapse or disruption.

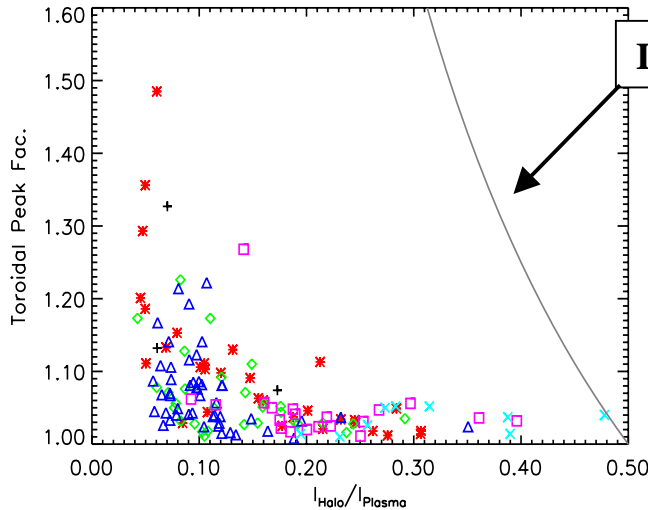
## 7. Halo currents in MAST

Spherical Tokamaks have good vertical stability at high 'natural' elongation ( $\kappa \sim 1.8$ , dependant upon current profile), where 'natural' means the elongation present in a uniform vertical field. A de-stabilising vertical field produces higher elongations which can lead to vertical displacement events (VDEs). Indeed many MAST discharges in this first campaign



ended in a VDE as the stray field from the (uncompensated) solenoid became increasingly destabilising as the discharge proceeded. Although theory and modelling predict that forces due to halo currents should be relatively low in the ST [7,8], it is important to verify this as MAST is designed for operation up to 2MA, and a comprehensive set of halo current diagnostics have been installed and commissioned [9].

Results to date are shown in Fig 13. It is seen that the currents (and forces) induced at a VDE are much lower than those met in tokamaks of conventional aspect ratio.

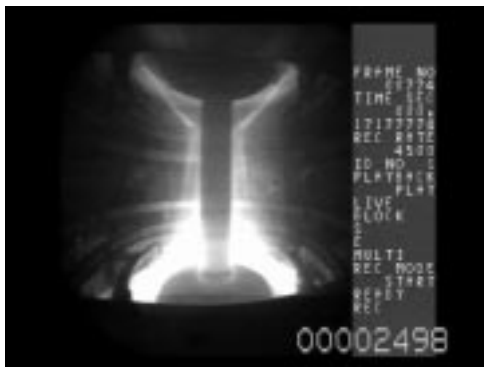


$$I_h/I_p \times TPF = 0.5$$

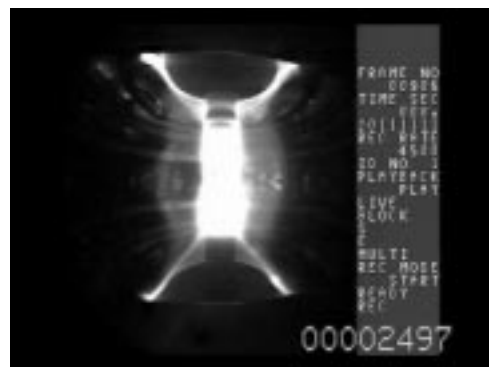
*Fig 13 Halo current fraction, and Toroidal Peaking Factor (TPF), calculated at time of maximum halo current. Line indicates typical design constraint for ITER-FEAT [10]; points having highest halo fractions are low current, higher aspect ratio discharges*

### 8. Current Terminations

Inspection of  $I_p$  waveforms and high-speed video recordings shows that many MAST discharges appear to end abruptly. Most of these events are actually VDEs, usually triggered by an IRE. At the end of the solenoid swing, the solenoid current is brought back to zero, producing a negative loop voltage, which causes changes in the plasma current profile and often an IRE. The combination of IRE, destabilising vertical field and unoptimised vertical feedback system often led to a VDE. In the next campaign it is intended to reduce the solenoid stray field by use of the P2 compensation coils and, with improvements in the vertical feedback system, most VDEs should be avoidable.



a) VDE



b) disruption

**Figure 14:** High-speed video stills of a VDE and a disruption.

It is important to know how susceptible STs are to other sorts of rapid termination. On START it was found that the plasma had a high degree of resilience to major disruptions [11]. In MAST, disruptions have not been observed during the current ramp-up phase, or when exploring the density limit (unless  $q_{95}$  is very low). Figure 14 shows comparisons of VDE and major disruption terminations on MAST. As can be seen, in a VDE the plasma moves abruptly up or down, whereas in a major disruption it remains in the mid-plane region.

High current MAST discharges do not disrupt directly: they suffer a series of IREs which reduce the current gradually, as shown in Fig 15, so that there is a range of possible points at which the plasma current (and other parameters) can be taken. The convention adopted is as shown in Fig 15, that parameters are measured at the last current dip before  $I_p$  goes to zero.

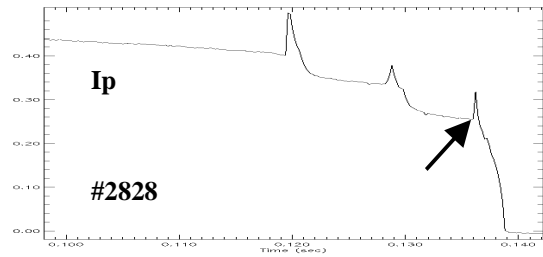


Fig 15 convention used for definition of disruption parameters

From the most recent 1198 shots, sixty non-VDE disruptions were found, with  $I_p$  between 40kA and 265kA. The final disruption is at lower current and, because the vertical field is not usually reduced accordingly, occurs where  $R$  is small and  $A$  is high ( figure 16). Of the disruptions at aspect ratios  $< 1.8$ , it is seen that all except two occur during the final ramp-down of plasma current. The higher current of these two shots is in #2828, shown in Fig 15.

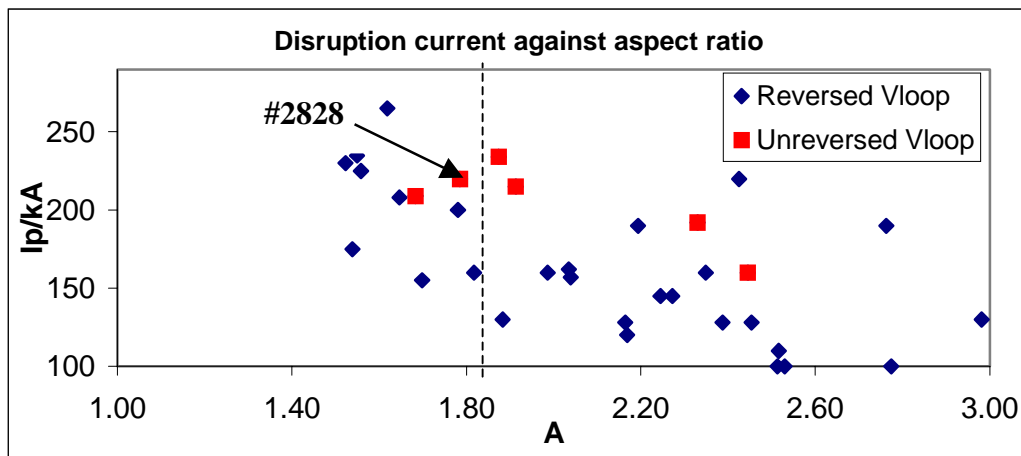


Figure 16: Plot of plasma current at disruption against aspect ratio. Disruptions for which  $V_{loop}$  is positive or zero are shown as red squares, others as blue diamonds. The dashed line at  $A=1.8$  divides disruptions in the ST regime from those in the non-ST regime.

These results suggest that MAST has indeed considerable resilience to the major disruption; moreover it is considered that this could be further improved by field control during the current ramp-down phase. It is noteworthy that in this first MAST campaign, a high-current termination only occurred if an IRE led to a vertical instability, as occurred for discharges 2700, 2701 shown in Fig 9. These may be avoidable by vertical field control and / or improved vertical feedback systems.

## 9. Divertor Power Loading studies in MAST

The SOL plasma parameters and power loadings in double-null (DND) ST geometry were measured and analysed for the first time on START [12], where several unusual features were observed, including strong in-out/up-down power asymmetries and significant SOL currents. However, analysis of the data was complicated by a blanket of high neutral density surrounding the START plasma (a result of the fuelling scheme, fully open divertor geometry and large vessel to plasma volume ratio), which was believed to give rise to large charge exchange losses from the SOL.

MAST is well equipped with arrays of high spatial resolution, swept Langmuir probe arrays (576 probes in total) covering all four strike point regions [13] (Fig. 17). For Ohmic plasmas, densities and temperatures in both the outboard and inboard SOLs produce strongly collisional conditions ( $v^* > 7$  and 50 respectively) with mid-plane heat flux density scale lengths of order 6mm at both positions. All the plasma parameter scale lengths are significantly broadened on the outboard side as a result of strong poloidal flux expansion ( $f_{exp} > 7$ ) (Fig 18).

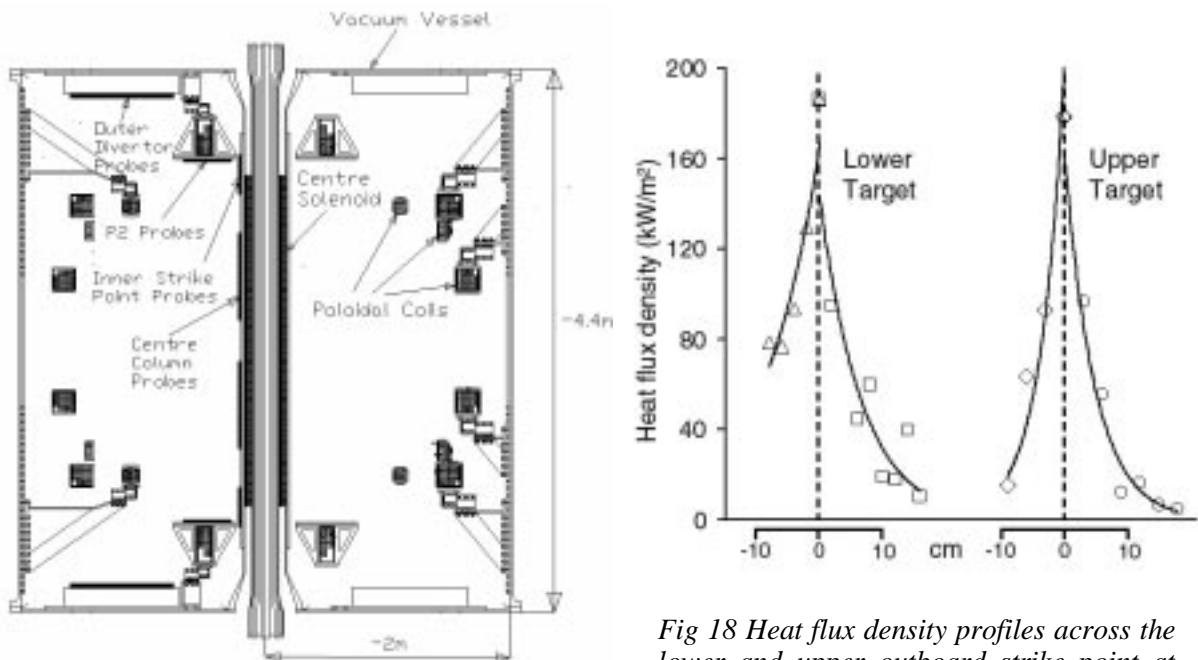


Fig 17 Location of Langmuir probes (576 in all) in MAST

Fig 18 Heat flux density profiles across the lower and upper outboard strike point at time 144 ms for shot 2321. Left hand side of the separatrix (dotted line) is the SOL, right hand side the private flux region

About two thirds of the power entering the SOL reached the targets compared to one third on START (the difference probably arising from higher charge exchange losses in START). The ratio of the average power to the outboard targets to the average power to the inboard targets was  $\sim 6.5 : 1$ . Since this exceeds the ratio of  $\sim 3 : 1$  for the outboard and inboard separatrix surface areas, the power loading on the inboard strike point may not be as critical for the ST as was initially supposed.

## 10. Conclusions

The first 6 months of MAST operations have been remarkably successful. Operationally, both merging-compression and the more conventional solenoid induction schemes have been demonstrated, the former providing over 400kA of plasma current with no demand on solenoid flux. Good vacuum and operational conditions, particularly after boronisation with trimethyl boron, have enabled the attainment of plasma current of over 1MA with central plasma temperatures (Ohmic) of order 1keV. The Hugill and Greenwald limits can be significantly exceeded, and H-mode achieved at modest additional NBI power. Moreover, particle and energy confinement show an immediate increase at the L-H transition, unlike on START where this only became apparent at the highest plasma currents. Halo currents are small, with low toroidal peaking factors, in accordance with theoretical predictions, and there is evidence of a resilience to the major disruption. These results, together with those from the other new STs now commencing operation, will rapidly increase understanding of the physics properties of the ST and determine its potential for a future fusion device.

## Acknowledgement

This work is funded jointly by the UK Department of Trade and Industry and EURATOM. The NBI equipment is on loan from ORNL, the NPA from PPPL, and EFIT is supplied by General Atomics.

## References

- [1] SYKES, A., et al, "The spherical tokamak programme at Culham", Nuclear Fusion **39**, 1271 (1999)
- [2] AKERS, R. et al, "Neutral Beam Heating of Spherical Tokamak Plasmas", this conf.
- [3] GRYAZNEVICH, M., "First results from MAST", 27th Eur. Conf. Contr. Fusion and Plasma Physics, Budapest, June 2000
- [4] SNIPES, J A, Proc. 24th EPS Conf. Controlled Fusion and Plasma Physics **21A**, III, p961 Berchtesgaden 1997
- [5] SYKES, A., AKERS, R., APPEL, L., CAROLAN, P.G et al, "H-mode operation in the START spherical tokamak", Phys. Rev. Lett. **84**, 495 (2000)
- [6] Yu.Dnestrovskij, M.P.Gryaznevich, A.Yu.Dnestrovskij, J.W.Connor et al, "Simulation of START Shots with the Canonical Profile Transport Model", Plasma Physics Reports, v.26,No 7, 2000, p.539.
- [7] CALOUTSIS, A and GIMBLETT, C G, UKAEA FUS 393 (1998), Nuclear Fusion **38** p1487
- [8] POMPHREY, N, BIALEK, J M & PARK, W, Nuclear Fusion **38** (1998) 449.
- [9] MARTIN, R., BUTTERY, R.J., CUNNINGHAM, G.C., FIELDING, S.J., et al, "Operation limits, VDEs and Halo currents on MAST", 27th Eur. Conf. Contr. Fusion and Plasma Physics, Budapest, June 2000, P1.041
- [10] YOSHINO, R., *et al.*, Proc.17th IAEA Conf. on fusion energy, Yokohama, Oct.1998. Paper ITERP1/14
- [11] SYKES, A., Phys. Plasmas **4** (1998) p1665
- [12] MOREL, K.M. et al, J. Nucl. Mater., 266-269 (1999) 1040 – 1044
- [13] COUNSELL, G.F., AHN, J-W., FIELDING, S.J., and MADDISON, G.P., "Divertor power loading studies in the MAST tokamak", 27th Eur. Conf. Contr. Fusion and Plasma Physics, Budapest, June 2000, P4.088